THE JOURNAL OF BIOLOGICAL CHEMISTRY VOL. 291, NO. 26, pp. 13622–13633, June 24, 2016

Identification and Functional Characterization of a Novel OprD-like Chitin Uptake Channel in Non-chitinolytic Bacteria*

Received for publication, March 22, 2016, and in revised form, April 22, 2016 Published, JBC Papers in Press, May 12, 2016, DOI 10.1074/jbc.M116.728881

H. Sasimali M. Soysa[‡1] **and Wipa Suginta**[‡§2]

From the [‡]*Biochemistry-Electrochemistry Research Unit and School of Chemistry, Institute of Science and* [§]*Center of Excellence in Advanced Functional Materials, Suranaree University of Technology, Nakhon Ratchasima 30000, Thailand*

Chitoporin from the chitinolytic marine *Vibrio* has been characterized as a trimeric OmpC-like channel responsible for effective chitin uptake. In this study we describe the identification and characterization of a novel OprD-like chitoporin (so-called *Ec*ChiP) from *Escherichia coli*. The gene was identified, cloned, and functionally expressed in the Omp-deficient *E. coli* BL21 (Omp8) Rosetta strain. On size exclusion chromatography, *Ec*ChiP had an apparent native molecular mass of 50 kDa, as predicted by amino acid sequencing and mass analysis, confirming that the protein is a monomer. Black lipid membrane reconstitution demonstrated that *Ec*ChiP could readily form stable, monomeric channels in artificial phospholipid membranes, with an average single channel conductance of 0.55 ± 0.01 nanosiemens and a slight preference for cations. Single *Ec*ChiP channels showed strong specificity, interacting with long chain chitooligosaccharides but not with maltooligosaccharides. Liposome swelling assays indicated the bulk permeation of neutral monosaccharides and showed the size exclusion limit of *Ec*ChiP to be ~200–300 Da for small permeants that pass through by general diffusion while allowing long chain chitooligosaccharides to pass through by a facilitated diffusion process. Taking *E. coli* as a model, we offer the first evidence that non-chitinolytic bacteria can activate a quiescent *ChiP* gene to express a functional chitoporin, enabling them to take up chitooligosaccharides for metabolism as an immediate source of energy.

Escherichia coli is a Gram-negative, heterotrophic bacterium that lives in open environments, such as soil, manure, and water, but the persistence of *E. coli* populations depends upon the availability of carbon substrates in each natural environment. *E. coli* usually grows on glucose-enriched nutrients such as starch, cellulose, and hemicellulose (1) but not on chitin polysaccharides as it intrinsically lacks competent chitin-utilization machinery (2, 3). The chitin degradation pathway is known to be highly active in marine *Vibrio*, the growth of which depends on the utilization of the chitin biomass as their sole source of cellular energy. The chitin degradation pathway of *Vibrio* incorporates a large number of chitin-degrading enzymes and transporters for chitooligosaccharides and *N*-acetyl glucosamine (4–6). Roseman and co-workers (6) first reported the identification and molecular cloning of the gene encoding chitoporin (*Vf*ChiP)[3] from *Vibrio furnissii*. *Vf*ChiP was expressed on induction with $(GlcNAc)_n$, $n = 2–6$, but was not induced by GlcNAc or by other sugars. In contrast to the parental strain, a mutant strain lacking *Vf*ChiP did not grow on $GlcNAc_3$, implying that *Vf*ChiP was selective for chitooligosaccharides (6). We recently identified and characterized the chitin uptake channel (so-called *Vh*ChiP) from the bioluminescent marine bacterium *Vibrio harveyi* (7, 8). *Vh*ChiP is a trimeric OmpC-like porin located in the outer membrane and responsible for the molecular uptake of chitin breakdown products that are generated by the action of secreted chitinases (4, 9–11). Single-channel recordings and liposome swelling assays confirmed that *Vh*ChiP is a sugar-specific channel that is particularly selective for chitooligosaccharides, chitohexaose having the greatest rate of translocation.

Unlike *Vibrio* species, the chitin catabolic cascade of non-chitinolytic bacteria, such as *Candida albicans* (12), *Xanthomonas campestris* (13), *Shewanella oneidensis* (14), and *E. coli* (15–17) was innately inactive although presumed to be preserved. Yang *et al.* (14) proposed the three-step biochemical conversion of GlcNAc (the monomer of chitin) to fructose 6-phosphate in *E. coli* through sequential phosphorylation, deacetylation, and isomerization-deamination reactions. The gene *ChiP* (formerly *ybfM*) encoding chitoporin was previously identified in *E. coli* and *Salmonella* sp. as a silent gene controlled by a non-coding small RNA (16). However, this *ChiP* gene was sporadically expressed as an adaptive strategy for the bacterium to thrive in glucose-deficient environments (16, 18–21). To date, *E. coli* chitoporin (so-called *Ec*ChiP) has not been functionally characterized, and our study used electrophysiological and biochemical approaches to uncover the physiological roles of *Ec*ChiP.

Experimental Procedures

Bacterial Strains and Vectors—E. coli strain DH5α, used for routine cloning and plasmid preparations, was obtained from Invitrogen. *E. coli* BL21(DE3) Omp8 Rosetta (Δ*lamBompF*::

* This work was supported by Suranaree University of Technology and the Office of the Higher Education Commission under the National Research University project of Thailand. The authors declare that they have no conflicts of interest with the contents of this article.

[1] Supported by Suranaree University of Technology through a SUT-OGRG grant.

[2] Supported by the Thailand Research Fund and Suranaree University of Technology through Basic Research Grant BRG578001 and Suranaree University of Technology Grants SUT1-102-57-36-18 and SUT1–102-59–12-17. To whom correspondence should be addressed. E-mail: wipa@sut.ac.th.

[3] The abbreviations used are: *Vf*ChiP, *V. furnissii* chitoporin; *Ec*ChiP, *E. coli* chitoporin; IPTG, isopropyl 1-thio-β-D-galactopyranoside; BLM, black lipid membrane; $GlcNAc_2$, chitobiose; $GlcNAc_3$, chitotriose; $GlcNAc_4$, chitotetraose; $GlcNAc_5$, chitopentaose; $GlcNAc_6$,chitohexaose; nS, nanosiemen(s).

Tn*5* Δ*ompA*Δ*ompC*) mutant strain was a gift from Professor Dr. Roland Benz, Jacobs University, Bremen, Germany. The pET23d(+) expression vector was a product of Novagen (Merck). pUC57 vector carrying the *E. coli ChiP* gene was obtained from GenScript USA Inc. Piscataway, NJ.

Chitosugars—Chitooligosaccharides, including chitobiose, chitotriose, chitotetraose, chitopentaose, and chitohexaose were purchased from Dextra Laboratories (Science and Technology Centre, Reading, United Kingdom).

Structural Prediction and Sequence Analysis—Amino acid sequences of four bacterial ChiPs from *E. coli* (P75733), *Salmonella* (Q7CQY4), *Serratia marcescens* (L7ZIP1), and *V. harveyi* (L0RVU0) were aligned and displayed using the program CLC Main Workbench v6.0. The secondary structure of the *E. coli* ChiP was constructed by ESPript 3.0 (22) according to the three-dimensional structure of *Pseudomonas aeruginosa* OprD (pdb 2odj).

Cloning and Sequencing—The nucleotide sequence encoding chitoporin was identified in the *E. coli* strain K-12 substrain MG1655 chromosome in the NCBI database (gi 49175990), and the *ChiP* gene was commercially synthesized using the GenScript Gene Synthesis Service. The ChiP DNA fragment ligated in the pUC57 cloning vector was excised and then transferred into the pET23d(+) expression vector using the NcoI and XhoI cloning sites so that the *ChiP* gene could be expressed under the control of the T7 promoter. The oligonucleotides used for colony detection of the ChiP PCR product were 5′-ATACCATGGCCATGCGTACGTTTAGT-3′ for the forward primer and 5′-AACCTCGAGTCAGAAGATGGTGAA-3′ for the reverse primer (sequences underlined indicate the restriction sites). Nucleotide sequences of sense and antisense strands of the PCR fragment were determined by automated sequencing (First BASE Laboratories SdnBhd, Selangor DarulEhsan, Malaysia).

Protein Expression and Purification—Expression and purification of the recombinant *Ec*ChiP were carried out as previously described (8). Briefly, the expression vector pET23d(+), harboring the full-length *ChiP* gene, was transformed into *E. coli* BL21(DE3) Omp8 Rosetta strain, which lacks major endogenous Omps, including OmpF, OmpC, OmpA, and LamB. The transformed cells were grown at 37 °C in Luria-Bertani (LB) broth supplemented with 100 $\mu g \cdot ml^{-1}$ ampicillin and 25 $\mu g \cdot ml^{-1}$ kanamycin. During the exponential growth phase ($A_{600} \sim 0.6-0.8$), *Ec*ChiP expression was induced with 0.5 mM final concentration of isopropyl thio-β-D-galactoside (IPTG). After 6 h of additional incubation at 37 °C, the cell pellet was harvested by centrifugation at 2,948 × *g* for 20 min at 4 °C.

For protein purification, the cell pellet was resuspended in lysis buffer (20 mM Tris-HCl, pH 8.0, 2.5 mM $MgCl_2$, 0.1 mM $CaCl_2$) containing 10 $\mu g \cdot ml^{-1}$ RNase A and 10 $\mu g \cdot ml^{-1}$ DNase I. Cells were disrupted with a high speed ultrasonic processor (EmulsiFlex-C3, Avestin Europe, Mannheim, Germany) for 10 min. After this, 20% (w/v) SDS solution was added to obtain a final concentration of 2%, and the suspension was further incubated at 50 °C for 60 min with 300 rpm shaking to ensure complete lysis. Cell wall components were removed by centrifugation at 100,000 × *g* at 4 °C for 1 h. The pellet, containing recombinant *Ec*ChiP, was extracted twice with 2.5% (v/v) *n*-octylpolyoxyethylene (Alexis Biochemicals, Lausanne, Switzerland) in 20 mM phosphate buffer, pH 7.4, and centrifuged again. The supernatant was then dialyzed thoroughly against 20 mM phosphate buffer, pH 7.4, containing 0.2% (v/v) lauryldimethylamine oxide (Sigma).

To obtain protein of high purity, the solubilized *Ec*ChiP was subjected to ion-exchange chromatography using a Hitrap Q HP prepacked column (5 × 1 ml) connected to an ÄKTA Prime plus FPLC system (GE Healthcare). Bound proteins were eluted with a linear gradient of 0–1 M KCl in 20 mM phosphate buffer, pH 7.4, containing 0.2% (v/v) lauryldimethylamine oxide. The purity of the eluted fractions was confirmed by SDS-PAGE. Fractions containing *Ec*ChiP were pooled and subjected to size exclusion chromatography using a HiPrep 16/60 Sephacryl S-200 high resolution column. The purity of the *Ec*ChiP fractions obtained after the size exclusion step was verified by SDS-PAGE before they were pooled, and the protein concentration of the freshly prepared *Ec*ChiP was estimated using the Novagen BCA protein assay kit (EMD Chemicals Inc., San Diego, CA).

Peptide Mass Analysis by MALDI-TOF MS—The purified *Ec*ChiP was electrophoresed on a 12% polyacrylamide gel, and the *Ec*ChiP bands were excised and sent to BGI Tech Solutions (HongKong) Co. Ltd. for MALDI-TOF MS analysis. Briefly, protein in the gel was digested with trypsin and eluted to obtain a peptide mixture, then MALDI-TOF mass spectrographic analysis was performed, and the obtained peptide masses were identified using Mascot software v2.3.02.

Molecular Weight Determination of EcChiP—Standard proteins and dyes of known molecular weight were resolved on a HiPrep 26/60 Sephacryl S-300 HR column. Dextran-2000 was used to obtain the void volume (V_0), whereas DNP-lysine was used to calculate the volume of the stationary phase (V_i) and the elution volume of each protein sample, denoted as V_e. The elution of a protein sample was characterized by the distribution coefficient (K_d) derived as in Equation 1,

$$K_d = \frac{V_e - V_0}{V_i} \quad \text{(Eq. 1)}$$

A calibration curve was created by plotting K_d *versus* logarithmic values of the corresponding molecular weights of the standard proteins and was used to estimate the molecular weight of *Ec*ChiP. The standard proteins used in this experiment were ferritin (440 kDa), catalase (250 kDa), aldolase (158 kDa), bovine serum albumin (66 kDa), ovalbumin (43 kDa), carbonic anhydrase (29 kDa), and ribonuclease A (13.7 kDa).

Black Lipid Bilayer Measurements of Pore Conductance and Chitin Oligosaccharide Translocation—Black lipid membrane (BLM) reconstitution was carried out in electrolyte containing 1 M KCl and 20 mM HEPES, pH 7.5, at room temperature (25 °C). Solvent-free bilayer (Montal-Mueller type) formation was performed using 1,2-diphytanoyl-*sn*-glycero-3-phosphatidylcholine; Avanti Polar Lipids, Alabaster, AL). First, the aperture was prepainted with a few microliters of 1% (v/v) hexadecane in hexane, then a planar bilayer was formed across the aperture by lowering and raising the liquid level (23). Ionic currents were detected using Ag^+/AgCl electrodes with a patch-

clamp amplifier connected to a two-electrode bilayer headstage (PC-ONE plus PC-ONE-50; Dagan Corp., Minneapolis, MN). The BLM setup was operated within a Faraday cage on a vibration-dampening table with an A/D converter (LIH 1600, HEKA Elektronik, Lambrecht, Germany) and was operated using the software PULSE program (HEKA Elektronik, Lambrecht, Germany). One of the electrodes, immersed in 1 M KCl electrolyte on the *cis* side of the cuvette, was connected to ground, whereas the electrode on the *trans* side was connected to the amplifier head-stage. *Ec*ChiP was always added to the *cis* side of the cuvette. Conductance values were extracted from the current steps observed at different voltages after the addition of the protein. The ion selectivity of *Ec*ChiP was determined using different salt solutions, such as 1 M lithium chloride (LiCl), 1 M cesium chloride (CsCl), and 1 M potassium acetate (KAc).

To investigate sugar translocation, single *Ec*ChiP channels were reconstituted in the artificial lipid membrane as described earlier. To prevent multiple insertions during data acquisition, the protein solution in the chamber was gently diluted after the first insertion by sequential additions of the working electrolyte. Then the fully open *Ec*ChiP channel was titrated with distinct concentrations of different chitooligosaccharides: chitobiose ($GlcNAc_2$), chitotriose ($GlcNAc_3$), chitotetraose ($GlcNAc_4$), chitopentaose ($GlcNAc_5$) and chitohexaose ($GlcNAc_6$). Each sugar was added to the *cis* side of the chamber. Fluctuations of ion flow were observed as a result of sugar diffusion through the reconstituted channel and were usually recorded for 2 min at different transmembrane potentials. To test the substrate specificity of the channel toward chitooligosaccharides, maltodextrin sugars were used as controls.

Liposome Swelling Assay—The *Ec*ChiP- and *Vh*ChiP-reconstituted proteoliposomes were prepared as described elsewhere (24, 25). Soybean L-α-phosphatidylcholine (20 mg/ml, freshly prepared in chloroform) (Sigma) was used to form multilamellar liposomes. For the preparation of proteoliposomes, 200 ng of *Ec*ChiP was reconstituted into 200 μl of the liposome suspension by sonication, and then 17% (w/v) dextran (40kDa) was entrapped in the proteoliposomes. D-Raffinose solutions were prepared in phosphate buffer to obtain concentrations of 40, 50, 60, and 70 mM for determination of the isotonic solute concentration. This value was then used for the adjustment of the isotonic concentration for other solutes. To carry out a liposome-swelling assay, 25 μl of the proteoliposome suspension was added to 600 μl of sugar solution, and changes in absorbance at 500 nm were monitored immediately. The apparent absorbance change over the first 60 s was used to estimate the swelling rate (s^{-1}) following the equation $\varphi = (1/A_i)dA/dt$ in which φ is the swelling rate, A_i is the initial absorbance, and dA/dt is the rate of absorbance change during the first 60 s. The swelling rate for each sugar was normalized by setting the rate of L-arabinose (150 Da), the smallest sugar, to 100%. The values presented are averages from three to five independent determinations. Protein-free liposomes and proteoliposomes without sugars were used as negative controls. The sugars tested were D-glucose (180 Da), D-mannose (180 Da), D-galactose (180 Da), *N*-acetylglucosamine (GlcNAc) (221 Da), D-sucrose (342 Da), D-melezitose (522 Da), $GlcNAc_2$ (424 Da), $GlcNAc_3$ (628 Da), $GlcNAc_4$ (830 Da), $GlcNAc_5$ (1034 Da), $GlcNAc_6$ (1237 Da), and maltodextrins.

Results

Cloning, Sequence Analysis, and Structure Prediction—The availability of the nucleotide sequence in the genome of *E. coli* strain K-12 sub-strain MG1655, (complete genome NCBI reference sequence; NC_000913) allowed the putative amino acid sequence of *E. coli* ChiP (so-called *Ec*ChiP) to be identified. The full-length *ChiP* gene corresponding to *Ec*ChiP was synthesized commercially, for which the target gene was ligated into the NcoI and XhoI cloning sites of the pUC57 cloning vector (GenScript). The nucleotide sequence of the *ChiP* gene, comprising 1407 bps, was translated to a putative polypeptide of 468 amino acids, including the 26-amino acid signal sequence. The theoretical mass of the full-length *Ec*ChiP was 52,780 Da, with a predicted isoelectric point of 4.70.

Amino acid sequence comparison of *Ec*ChiP with other bacterial ChiPs in the SwissProt/UniProtKB database is presented in Fig. 1. The putative sequence of *Ec*ChiP showed highest sequence identity to *Salmonella typhimurium* ChiP (Q7CQY4) (90%) (18) followed by *S. marcescens* ChiP (L7ZIP1) (70%) (26). Our sequence analysis indicated that *Ec*ChiP had exceptionally low identity with the ChiP sequences from marine *Vibrio* species, such as *Vibrio cholerae* ChiP (Q9KTD0) (27), *V. furnissii* ChiP (Q9KK91) (6), and *V. harveyi* ChiP (L0RVU0) (8) with 13, 14, and 12% identity, respectively. Unlike marine *Vibrio* species, *E. coli* and S. *typhimurium* are non-chitinolytic bacteria that possess ChiP homologs belonging to the OprD family of porins. The *Ec*ChiP amino acid sequence was submitted to the Swiss-model database for homology structure prediction, and the crystal structure of *P. aeruginosa* OprD (pdb 2odj) (28) was computationally selected as a structure template. Fig. 2*A* shows a side view of the predicted β-barrel structure of *Ec*ChiP, atypically consisting of 19-strands connected by 9 external loops and 9 periplasmic turns. Previous reports of the crystal structures of the maltoporin (LamB) (29) and sucrose-specific porin ScrY (30) suggested that aromatic residues are important for sugar transport. Amino acid residues located within the pore interior, such as Trp-138, Asp-314, Arg-320, and Tyr-421, are predicted to be crucial for sugar transport (residues marked as sticks in Fig. 2*B*, top view). The predicted transmembrane topology for *Ec*ChiP is shown in Fig. 2*C*. The longest loop (L3, Gly-124 to Tyr-145) found inside the channel lumen presumably acts as the pore-confining loop that controls ion flow.

Recombinant Expression, Purification, and Mass Identification—The plasmid pET23d(+) harboring the *ChiP* gene fragment was designed to express recombinant *Ec*ChiP, with the 26-amino acid N-terminal signal sequence aiding channel insertion into the cell wall of the *E. coli* BL21(DE3) Omp8 Rosetta host. When the transformed cells were grown to exponential phase, expression of the recombinant *Ec*ChiP was induced with 0.5 mM IPTG for a period of 6h at 37 °C. Fig. 3*A* shows SDS-PAGE analysis of whole cell lysates of the Omp-deficient *E. coli* expressing *Ec*ChiP. When compared with cells transformed with the empty vector (*lane 1*, no induction; and *lane 2*, IPTG induction), uninduced cells transformed with the pET23d(+)/*ChiP* vector did not produce the heterologous pro-

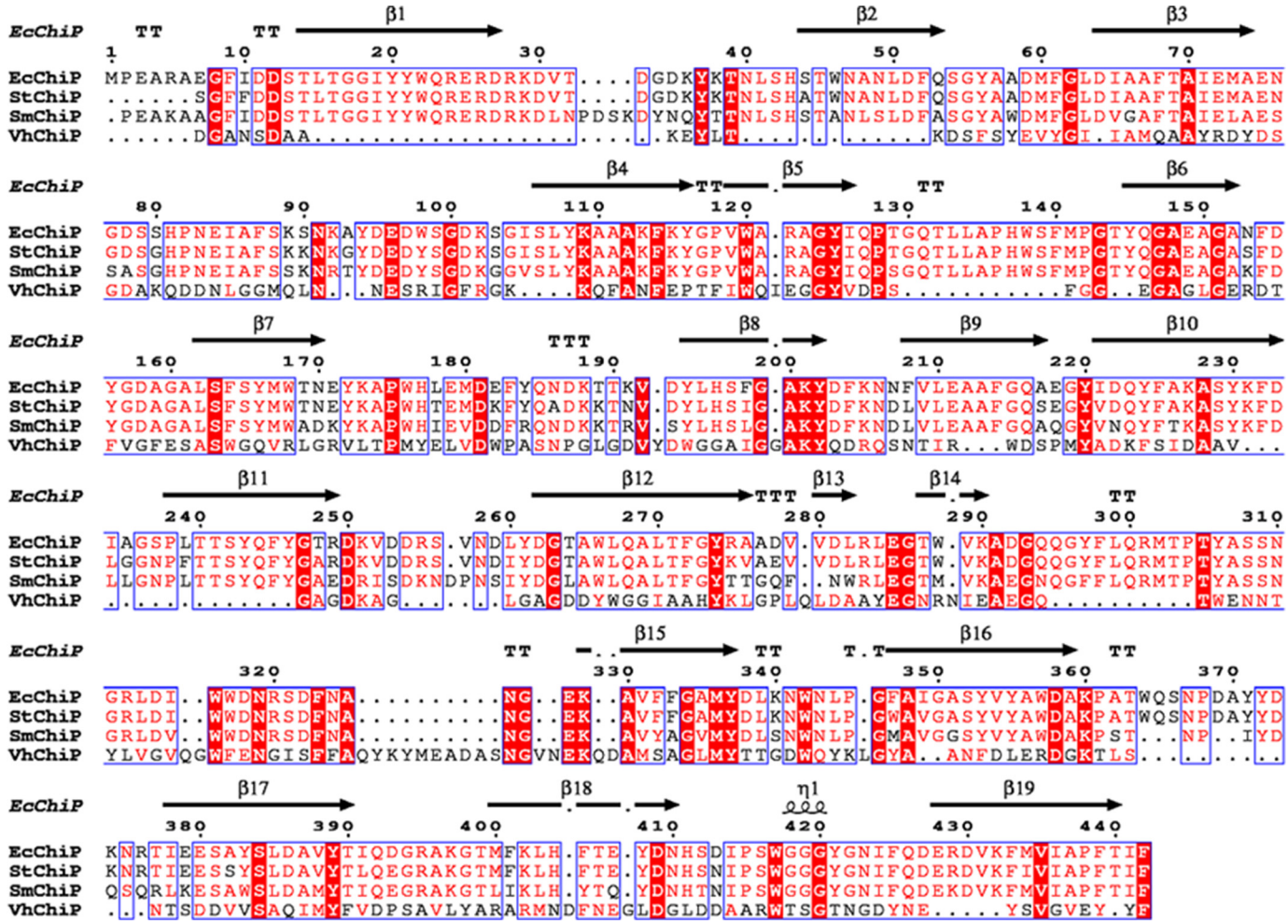

FIGURE 1. **Sequence alignment of *Ec*ChiP, showing the secondary structural elements of *Ec*ChiP.** The amino acid sequences of S. *typhimurium ChiP* (*StChiP*), *S. marcescens* ChiP (*SmChiP*), and *V. harveyi* ChiP (*VhChiP*), without signal peptides, were aligned using CLC Main Workbench 6. The secondary structure of *E. coli* was constructed by ESPript 3.0 according to the structure of *P. aeruginosa* OprD (pdb 2odj). β-Strands are marked with *black arrows*, and an α-helix is marked with *black curl*. Absolutely conserved residues are highlighted in *red*.

tein (*lane 3*), whereas a prominent band of the expected size (50 kDa) appeared on induction with IPTG (*lane 4*). These results confirmed successful production of *Ec*ChiP in the selected host cells.

For purification of *Ec*ChiP, the induced cells were subjected to a two-step detergent extraction. In the first step using 2% (w/v) SDS, most of *Ec*ChiP remained in the insoluble fraction, and in the second step *Ec*ChiP was solubilized with 2.5% (v/v) *n*-octylpolyoxyethylene. The protein purity observed after these steps was >90%. *Ec*ChiP was further subjected to ion-exchange chromatography using a Hitrap Q HP pre-packed column. Fig. 3*B* shows the chromatographic profile, indicating that *Ec*ChiP fractions were eluted in two peaks (P1 and P2) by an applied gradient of 0–1 M KCl. SDS-PAGE analysis shows that the *Ec*ChiP fractions in the first peak (P1) were highly purified (Fig. 3*B*, *inset*), whereas the fractions in P2 included some contaminants (not shown); P2 may, therefore, contain *Ec*ChiP bound to other proteins. Peaks P1 and P2 were, therefore, applied separately to a HiPrep 16/60 Sephacryl S-200 high resolution exclusion chromatography column for final purification. The highly purified *Ec*ChiP obtained after gel filtration chromatography was subjected to in-gel digestion for MALDI-TOF MS analysis. A MASCOT database search identified 16 peptides (designated P1-P16) that belonged to the internal sequences of the putative chitoporin from *E. coli* (gi 251784171 ref YP_002998475.1) (Fig. 3*C*, sequences in *cyan*). The sequence coverage for the identified peptides was 50%. These results confirmed that the 50-kDa protein expressed in *E. coli* BL21(DE3) Omp8 Rosetta host was *Ec*ChiP.

Determination of the Native State of the EcChiP Channel—All chitoporins identified in marine *Vibrio* species are trimeric channels (8). In the next series of experiments we investigated the native state of *Ec*ChiP. Unlike *Vh*ChiP (8), *Ec*ChiP did not migrate on SDS-PAGE gel to the position corresponding to a trimer under non-denaturing conditions. Fig. 4*A* is an SDS-PAGE analysis showing the migrations of *Vh*ChiP (*lane 1*, unheated; *lane 2*, heated) and *Ec*ChiP (*lane 3*, unheated; *lane 4*, heated). Intact *Vh*ChiP migrated with an apparent molecular mass close to 100 kDa, indicating a trimer (*lane 1*), but the dissociated subunits migrated close to 40 kDa (*lane 2*). Different results were observed with the *E. coli* sample; native *Ec*ChiP migrated with an apparent molecular mass of ~35 kDa (*lane 3*), indicating a monomeric, folded structure according to litera-

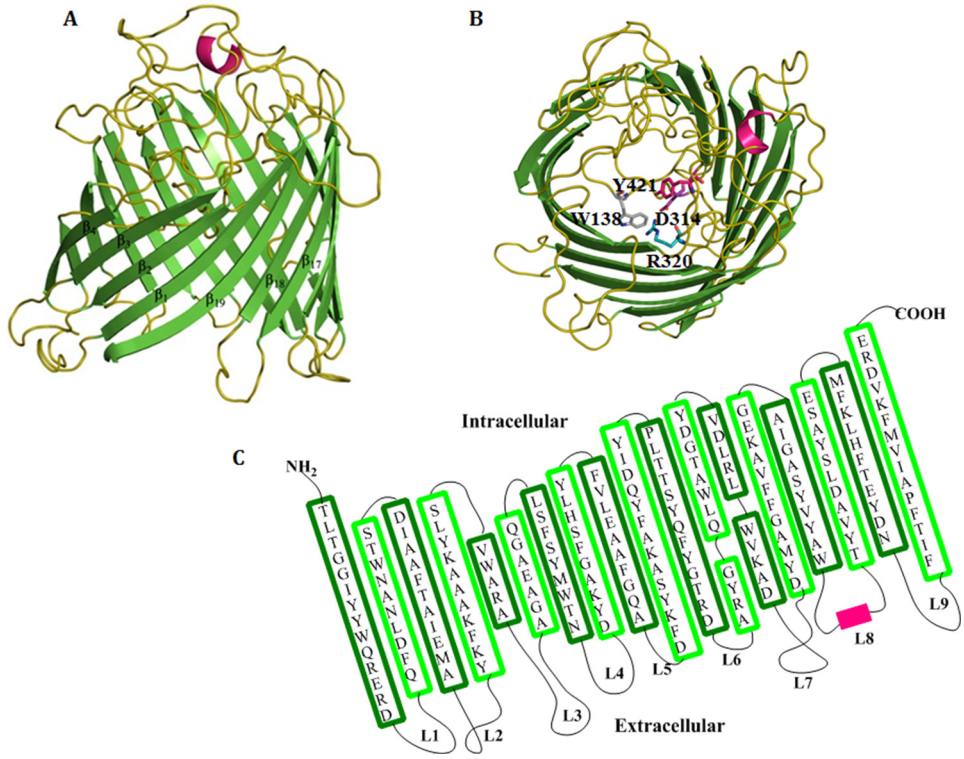

FIGURE 2. **The Swiss-model structure of *E. coli* chitoporin.** *A*, schematic of *Ec*ChiP viewed from the side. *B*, top view of the *Ec*ChiP modeled structure. Important residues in the pore that may be involved in sugar transport; Trp-138, Asp-314, Arg-320, and Tyr-421 are presented in *gray*, *purple*, *teal*, and *pink*, respectively, as stick structures. The x-ray structure of OprD from *P. aeruginosa* (pdb 2odj) was selected as the structure template for *E. coli* chitoporins. *Green*, β-strands; *olive*, loops and turns; *hot pink*, α-helices. *C*, the predicted transmembrane topology of *Ec*ChiP.

ture review (31, 32). After boiling, the apparent molecular mass increased to nearly 50 kDa, presumably due to unfolding of the protein (*lane 4*). Gel filtration chromatography was used to confirm the monomeric structure of native *Ec*ChiP. Fig. 4*B* shows a chromatographic profile of the protein standards eluted from a HiPrep 26/60 Sephacryl S-300 pre-packed column. *Ec*ChiP was eluted at a position between ovalbumin (43 kDa) and bovine serum albumin (66 kDa) (Fig. 4*B*, *black dotted line*), and its apparent molecular mass estimated from its distribution coefficient (K_d) was *ca.* 60 kDa (Fig. 4*C*), consistent with a monomeric molecule. The slightly greater molecular mass than the expected size of *Ec*ChiP (50 kDa) may be added by the molecular mass the detergent lauryldimethylamine oxide (micelle molecular mass 17 kDa) (33), which was included to maintain the protein solubility.

Channel-forming Properties of EcChiP—To examine the pore-forming properties of the isolated channel, *Ec*ChiP was reconstituted into artificial planar phospholipid membranes. An abrupt increase in ion current in response to an externally applied potential was observed soon after the addition of the protein, and the induced current remained steady throughout the subsequent period of data acquisition (usually 2 min). The BLM results clearly demonstrated that *Ec*ChiP was a channel-forming protein. Fig. 5*A* is a representative ion current recording of ~50 pA at +100 mV, signifying a characteristic single *Ec*ChiP insertion under a given condition (<2 ng·ml^{-1} *Ec*ChiP added on the *cis* side of the chamber filled with 1 M KCl, pH 7.5). This channel insertion behavior was observed consistently throughout our study. In Fig. 5*B*, we show typical ion current traces obtained from multiple insertions in the presence of a high added concentration of *Ec*ChiP (>10 ng·ml^{-1}) in the same electrolyte solution. The Fig. 5*B inset* shows the Gaussian distribution of the pore conductance, derived from 365 channel insertions. The value was fitted with a mean conductance of 0.54 ± 0.04 nS, which corresponded well with the value obtained from the slope of the I-V curve shown in Fig. 5*C*, *inset*. For individual *Ec*ChiP channels, currents were recorded at potentials from −100 to +100 mV, increased in 25-mV steps, as shown in Fig. 5*C*. The plot of current as a function of transmembrane potential was constructed from 17 independent single channel insertions. The conductance of the pore (slope of the curve) was constant over the entire voltage range scanned, yielding the conductance value of 0.55 ± 0.01 nS. *Ec*ChiP was shown to be a relatively stable channel at both negative and positive potentials with a threshold for channel gating observed at approximately −200 mV and +200 mV. An example of channel gating at +200 mV is shown in Fig. 5*D*.

Single-channel experiments were also performed with salts other than KCl to obtain information on the ion selectivity of *Ec*ChiP; the results are summarized in Table 1. Replacement of Cl^- by CH_3COO^-, a less mobile anion, slightly reduced the single channel conductance from 0.5 to 0.4 nS. However, replacement of K^+ by the less mobile cation Li^+ resulted in a much larger decrease, from 0.5 nS to 0.25 nS, indicating a preference of *Ec*ChiP for cations (Table 1). Although Li^+ and CH_3COO^- and K^+ and Cl^- have similar aqueous mobilities (34, 35), the conductance of *Ec*ChiP channel was lower in LiCl

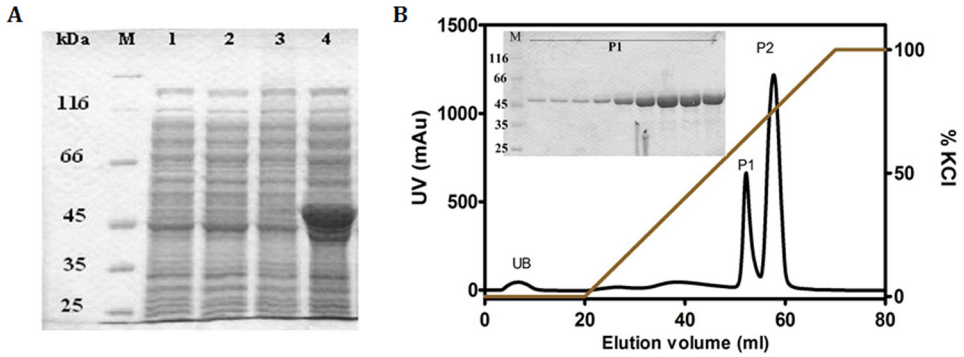

C

<u>MRTFSGKRSTLALAIAGVTAMSGFMA</u>MPEARAEGFIDDSTLTGGIYYWQRER

DRKDVTDGDKYKTNLSHSTWNANLDFQSGYAADMFGLDIAAFTAIEMAENGDS

SHPNEIAFSKSNKAYDEDWSGDKSGISLYKAAAKFKYGPVWARAGYIQPTGQTL

LAPHWSFMPGTYQGAEAGANFDYGDAGALSFSYMWTNEYKAPWHLEMDEFY

QNDKTTKVDYLHSFGAKYDFKNNFVLEAAFGQAEGYIDQYFAKASYKFDIAGSP

LTTSYQFYGTRDKVDDRSVNDLYDGTAWLQALTFGYRAADVVDLRLEGTWVK

ADGQQGYFLQRMTPTYASSNGRLDIWWDNRSDFNANGEKAVFFGAMYDLKN

WNLPGFAIGASYVYAWDAKPATWQSNPDAYYDKNRTIEESAYSLDAVYTIQDG

RAKGTMFKLHFTEYDNHSDIPSWGGGYGNIFQDERDVKFMVIAPFTIF

FIGURE 3. **Recombinant expression, purification, and mass identification.** *A*, SDS-PAGE analysis of whole-cell lysate with and without IPTG induction for *E. coli* carrying pET23d(+) and pET23d(+)/*Ec*ChiP. *Lane M*, marker proteins; *lane 1*, *E. coli* Omp8 Rosetta carrying pET23d(+) without IPTG induction; *lane 2*, *E. coli* Omp8 Rosetta carrying pET23d(+) with IPTG induction; *lane 3*, *E. coli* Omp8 Rosetta carrying pET23d(+)/*Ec*ChiP without IPTG induction; *lane 4*, *E. coli* Omp8 Rosetta carrying pET23d(+)/*Ec*ChiP with IPTG induction. *B*, chromatographic profile of *Ec*ChiP purification with a Hitrap Q HP prepacked column (5 × 1 ml) connected to an ÄKTA Prime plus FPLC system. Bound proteins were eluted with a linear gradient of 0–1 M KCl in 20 mM phosphate buffer, pH 7.4, containing 0.2% (v/v) lauryldimethylamine oxide. SDS-PAGE analysis of bound fraction P1 is shown in an *inset*. *mAu*, milliabsorbance units. *C*, identification of tryptic digests of the expressed proteins by MALDI-TOF MS. The 16 identified peptides (P1-P16) that gave a complete match with putative peptides of *Ec*ChiP are shown in *cyan*. The N-terminal ends of peptides P2, P5, P6, P7, P8, P9, P10, P11, P12, P13, and P14 are indicated by *asterisks*. The 26-amino acid signal peptide is in *bold* and *underlined*.

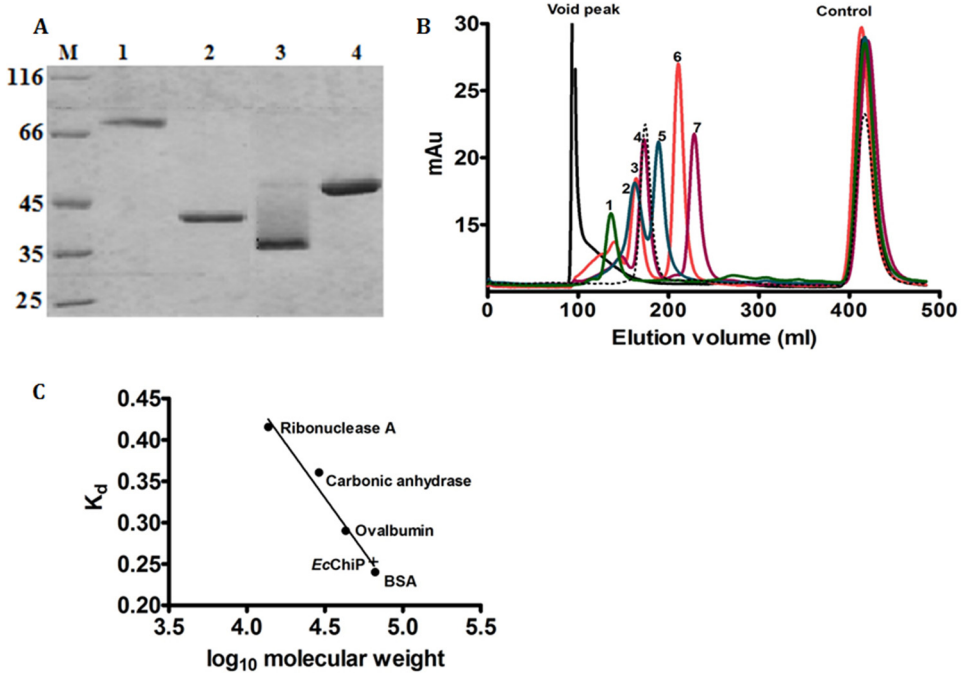

FIGURE 4. **SDS-PAGE analysis of *Ec*ChiP and molecular weight determination.** *A*, SDS-PAGE analysis of purified *Ec*ChiP, with *Vh*ChiP for comparison. *Lane M*, marker proteins; *Lane 1*,*Vh*ChiP (unheated); *lane 2*, *Vh*ChiP (heated); *lane 3*, *Ec*ChiP (unheated); *lane 4*, *Ec*ChiP (heated). *B*, size exclusion chromatogram of standard proteins with *Ec*ChiP. Standards were run separately, together with DNP-lysine (control). Protein standards: *lane 1*, ferritin (440 kDa); *lane 2*, catalase (250 kDa); *lane 3*, aldolase (158 kDa); *lane 4*, bovine serum albumin (66 kDa); *lane 5*, ovalbumin (43 kDa); *lane 6*, carbonic anhydrase (29 kDa); *lane 7*, ribonuclease A (13.7 kDa). *Void peak*, elution peak of blue dextran 2000. *Control*, elution peak for DNP-lysine. *Ec*ChiP was eluted (*black dotted line*) as a monomer within the 43–66 kDa range. *C*, calibration curve to determine the K_d value of *Ec*ChiP.

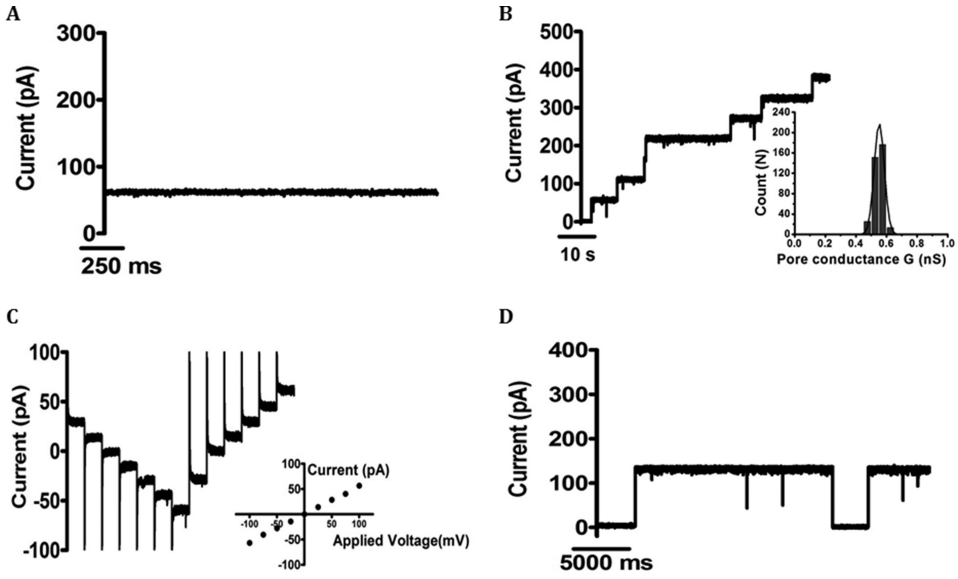

FIGURE 5. **Single-channel recordings of *Ec*ChiP in artificial lipid membranes.** Lipid bilayers were formed across a 70 μM aperture by the lowering and raising technique, using 5 mg·ml^{-1} 1,2-diphytanoyl-*sn*-glycero-3-phosphatidylcholine in *n*-pentane and 1 M KCl in 20 mM HEPES, pH 7.5, on both sides of the chamber. The protein was added to the *cis* side. *A*, fully open *Ec*ChiP current trace at +100 mV. *B*, multiple channel insertions; *Inset*, histogram of the conductance steps observed with 1,2-diphytanoyl-*sn*-glycero-3-phosphatidylcholine artificial bilayer for 365 independent channel insertions. The *black line* represents a single Gaussian fit. *C*, stepwise ramping of the potential for single insertion. *Inset*, I-V plot for a single *Ec*ChiP single channel. The average current values were obtained by varying the potential from −100 mV to +100 mV in 25 mV steps for 17 independent channel insertions. *D*, gating behavior of *Ec*ChiP at high potential (+200 mV).

TABLE 1

Average single channel conductance (G) of *Ec*ChiP in different salt solutions

The pH of the aqueous salt solutions was around 7.5. G was calculated from the single channel recording by averaging single events as indicated within the parentheses. The applied membrane potential was +100 mV.

Aqueous salt solution	Single channel conductance (G)
	nS
1 M KCl	0.54 ± 0.04 (n = 365)[a]
1 M KAc	0.40 ± 0.03 (n = 71)
1 M CsCl	0.60 ± 0.04 (n = 87)
1 M LiCl	0.25 ± 0.02 (n = 65)

[a] n represents the number of BLM measurements in which the data were acquired in this experiment.

than in KAc. This result supports the conclusion that the *Ec*ChiP channel was cation-selective.

Investigation of Chitooligosaccharide Interactions with EcChiP—In this set of experiments we performed single-channel measurements in the presence of different chitooligosaccharides to address the substrate specificity of the newly isolated channel. Fig. 6*A* is a control trace, showing a stably opening channel of conductance ~55 pA at +100 mV in the absence of ligand. The addition of the chitooligosaccharides chitotetraose, pentaose, and hexaose resulted in frequent current blockages in *Ec*ChiP, reflecting strong sugar-channel interactions (Fig. 6, *E–G*). We observed no fluctuation of ion current on the addition of *N*-acetylglucosamine, chitobiose and chitotriose (Fig. 6, *B, C* and *D*), and addition of structurally related maltohexaose (Fig. 6*H*) showed no fluctuation of ion current even at a concentration 200-fold greater than that of the chitosugars, indicating that the *Ec*ChiP channel was highly specific for chitooligosaccharides.

LamB has been the subject of intensive studies on sugar binding (36–38). Similarly, our BLM data showed that *Ec*ChiP interacted with chitosugars to various extents depending on the sizes and the types of the sugars, as shown in Fig. 6. Next, we selected chitohexaose as a substrate to study ion current fluctuation at different sugar concentrations. Fig. 7 shows current recordings obtained from a single *Ec*ChiP channel in the presence of several discrete concentrations of chitohexaose. These traces, recorded at +100 mV, indicated increasing numbers of blocking events as concentrations of chitohexaose were increased from 1.25 to 20 μM, leading to a gradual reduction in the average conductance of the channel (Fig. 7, *A–D*). Similar results were obtained at −100 mV, with the channel more susceptible to sugar occlusion at negative voltages (Fig. 7, *E–H*). At the highest sugar concentration (20 μM), we observed that the sugar molecules fully occupied the channel, leading to more frequent decreases in ion current to zero (Fig. 7, *D* and *H*). We did not detect three-stage transient blockages with *Ec*ChiP measurements on sugar addition, which are usually observed for trimeric channels (8, 36–39). These results provide further evidence that *Ec*ChiP acts as a monomeric channel.

Determination of Channel Specificity Using a Liposome-swelling Assay—Proteoliposome swelling assays were performed to evaluate the bulk permeation of neutral solutes through the *Ec*ChiP channel. *Ec*ChiP-containing proteoliposomes were prepared according to the protocol described elsewhere (24, 25). Swelling of the proteoliposomes caused by diffusion of solute molecules through the protein channel resulted in a decrease in apparent absorbance at 500 nm, whereas under isotonic conditions constant absorbance was maintained. In this assay we used D-raffinose (504 Da), a branched sugar that is unable to diffuse through the porin, to establish the isotonic concentration and enable the comparison of diffusion rates. L-Arabinose (150 Da), the smallest sugar tested in this experiment, had the highest diffusion rate through *Ec*ChiP, and the

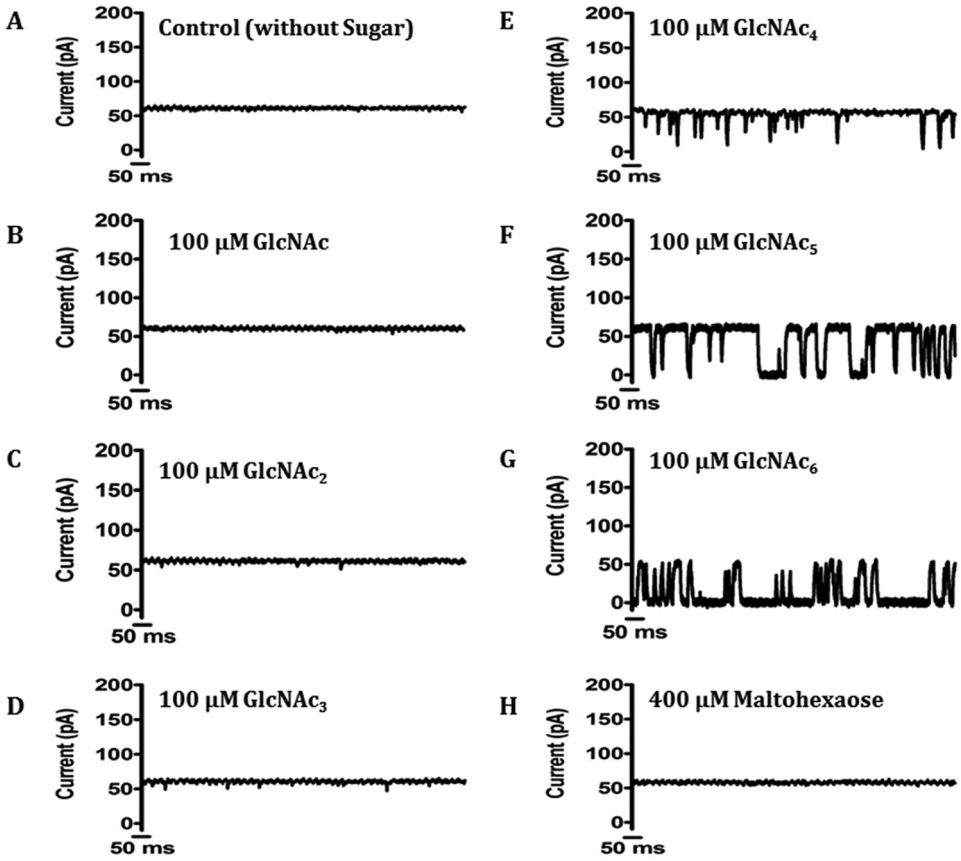

FIGURE 6. **Current recordings of single *Ec*ChiP channels in solutions of different chitooligosaccharides of various chain lengths.** Ion current fluctuations were monitored for 120 s at applied potentials of ±100mV. Here, only current traces for 1 s at +100 mV are presented. *A*, a fully open state of *Ec*ChiP before sugar addition. Then GlcNAc (*N*-acetylglucosamine) (*B*), chitobiose ($GlcNAc_2$) (*C*), chitotriose ($GlcNAc_3$) (*D*), chitotetraose ($GlcNAc_4$) (*E*), chitopentaose ($GlcNAc_5$) (*F*), or chitohexaose ($GlcNAc_6$) (*G*) were added on the *cis* side of the chamber to a final concentration of 100 μM. *H*, control recording with maltohexaose at a concentration of 400 μM.

swelling rates in the other sugars tested were normalized relative to that in L-arabinose, which was set to 100%.

To address the differences between the *Ec*ChiP channel and the chitooligosaccharide-specific porins from the OmpC family, we compared our data with those obtained with *Vh*ChiP-incorporating proteoliposomes. The two chitoporins showed similar diffusion rates for small sugars such as D-glucose, D-mannose, and D-galactose (180 Da) and *N*-acetylglucosamine (GlcNAc, 221 Da) (Fig. 8*A*). However, D-sucrose (342 Da), maltose (360 Da), and D-melezitose (522 Da) showed no diffusion through *Ec*ChiP. In contrast, D-sucrose and maltose permeated *Vh*ChiP, albeit with very low diffusion rates, whereas D-melezitose was impermeant. When *Ec*ChiP was tested with long chain chitooligosacharides it was found that all neutral chitooligosaccharides were permeant (Fig. 8*B*), whereas maltosugars (maltose and maltahexaose) did not show permeation. The results obtained from the proteoliposome swelling assays additionally confirmed the high selectivity of *Ec*ChiP for chitooligosaccharides.

Discussion

Chitin is one of the most abundant naturally occurring polysaccharides, and chitin turnover by marine *Vibrio* species is essential for the recycling of carbon and nitrogen in marine ecosystems (40). *Vibrio* species possess competent chitin degradation and uptake systems that allow the bacteria to metabolize chitinous materials, generating catabolic intermediates that can be used as their sole source of energy (5, 41–47). In marked contrast, *E. coli* is a non-chitinolytic bacterium living primarily in the gastrointestinal tract of animals, and its generation of cellular energy relies on glucose-enriched nutrients. Although the *ChiP* gene, encoding a chitoporin that is responsible for the uptake of chitin-derived chitooligosaccharides, is evolutionarily conserved, it is usually quiescent in non-chitinolytic bacteria. A previous report on *Salmonella* and *E. coli* (16, 18) showed that in the absence of any inducer, the *ChiP* gene (formerly *ybfM*) was constantly suppressed by forming a DNA-RNA duplex with a conserved small RNA, namely *ChiX*. However, silencing was relieved in the presence of chitooligosaccharides, as these sugars produced accumulation of anti-*ChiX* small RNA that paired with *ChiX*, allowing the *ChiP* gene to be expressed. Another study reported co-localization of the genes for *ChiP* and *Hex* (encoding β-*N*-acetylglucosaminidase) in the chromosomes of *Yersinia* and *Serratia* species (14). This suggested a sequential action of ChiP and β-*N*-acetylglucosaminidase in chitin uptake and chitin degradation, respectively, and *E. coli* and *Salmonella* ChiPs have been proposed to be involved in the uptake of chitobiose, an end product of chitin breakdown that is readily transported through the

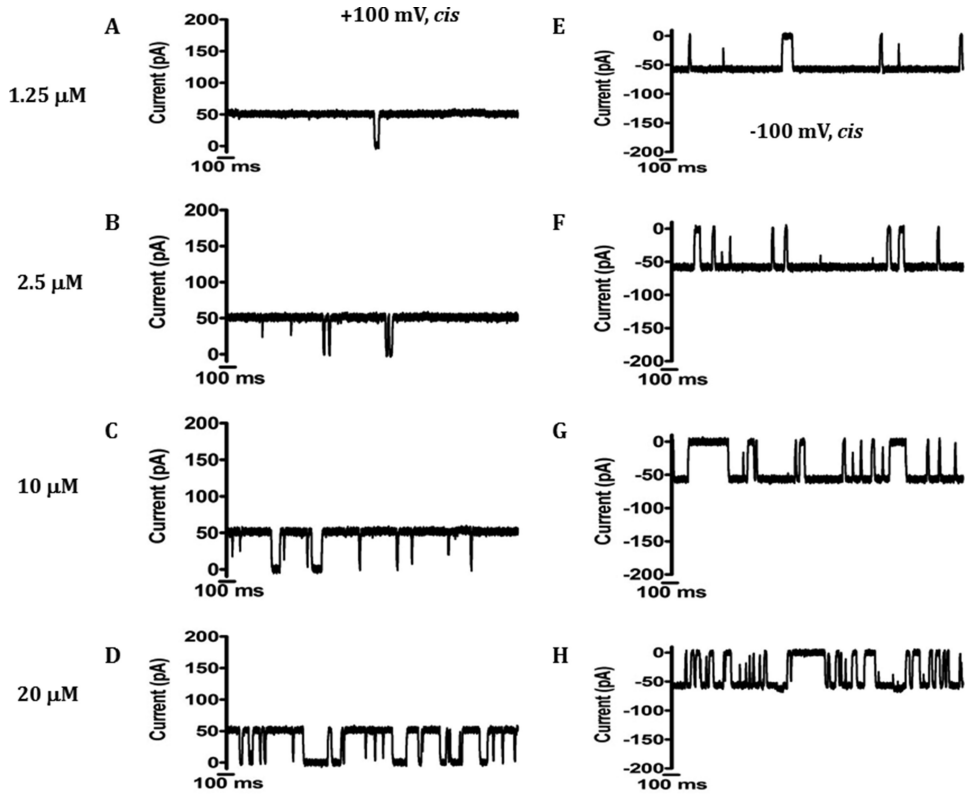

FIGURE 7. **Conductance of the same single *Ec*ChiP channel with increasing chitohexaose concentration at positive and negative potentials.** Ion current fluctuations were monitored for 120 s at applied potentials of ±100 mV with sugar addition on the *cis* side. Here only current traces for 2 s are presented with four different concentrations at +100mV (*A–D*) and at −100mV (*E–H*).

inner membrane by the phosphoenolpyruvate transferase system.

In the present study we identified the *ChiP* gene, encoding a hypothetical outer-membrane chitoporin (*Ec*ChiP) from the genome of the *E. coli* strain K-12, substrain MG1655. Amino acid sequence analysis showed that *Ec*ChiP had exceptionally low sequence identity (<14%) to all ChiPs from the OmpC family, such as *Vh*ChiP from *V. harveyi* and *Vf*ChiP from *V. furnissii* (6, 8). This suggested that the *ChiP* genes from *E. coli* and from *Vibrio* sp. did not share common ancestors, and further sequence analysis showed that *Ec*ChiP was similar to *Sm*ChiP from *S. marcescens* (75% identity), both of which are members of the OprD family.

The recombinant *Ec*ChiP displayed quite different channel behavior from other sugar-specific porins. Its most distinctive feature was that it formed a monomeric channel rather than the trimeric channel observed with other known ChiPs and that the channel was stably open over a wide range of external membrane potentials, with only occasional gating at high voltages (±200 mV). At 0.55 ± 0.01 nS, the single channel conductance of *Ec*ChiP was approximately ⅓ that of the well studied *Vh*ChiP (1.8 ± 0.3 nS) (8), consistent with our observation that *Ec*ChiP formed a monomeric channel, whereas *Vh*ChiP worked as a trimer. Comparison with the monomeric OprD from *P. aeruginosa*, a basic amino acid uptake channel (28), revealed that *P. aeruginosa* OprD had a narrow central constriction zone and displayed a much smaller conductance (28 pS) than that of *Ec*ChiP under the same electrolyte conditions (1 M KCl and pH 7.5). This suggests differences in the amino acids that line the channel interior and regulate the net ion flow in *Ec*ChiP as compared with those in OprD.

Measuring changes in ion flow upon varying the cationic/anionic species could provide some information regarding ion selectivity. For examples, Benz and co-workers (34, 35) used LiCl and KAc to test the channel selectivity of the maltodextrin-specific channel LamB and the glucose-inducible channel OprB. Both channels showed a preference for cations over anions. Following their method, our channel exhibited similar preference. We also measured the K^+/Cl^- selectivity by observing changes in reverse membrane potential at zero current under a 0.1–3.0 M gradient of KCl, yielding a P_c/P_a ratio of 2.8, which was slightly lower than the value obtained for the trimeric *Vh*ChiP ($P_c/P_a = 3.2$) (48). Nonetheless, the ion selectivity study obtained from both techniques confirmed that *Ec*ChiP was a cationic-selective channel.

We further examined sugar-channel interactions with various chitooligosaccharides. Our BLM data showed that *Ec*ChiP interacted strongly with long-chain chitooligosaccharides but not with maltooligosaccharides, implying that the channel was specific for chitooligosaccharide uptake. Strong interaction with the higher molecular weight substrates is also a characteristic of other sugar-specific channels, such as LamB (37, 38, 49), *Vh*ChiP (8, 48), and CymA (50). Consistent with this is an earlier *in vivo* study that showed no growth of *S. marcescens* expressing the null ChiP mutant in the presence of chitooligosaccharides larger than chitotriose (26). Both results confirmed the physiological roles of the OprD-related ChiP in chitooligosaccharide uptake.

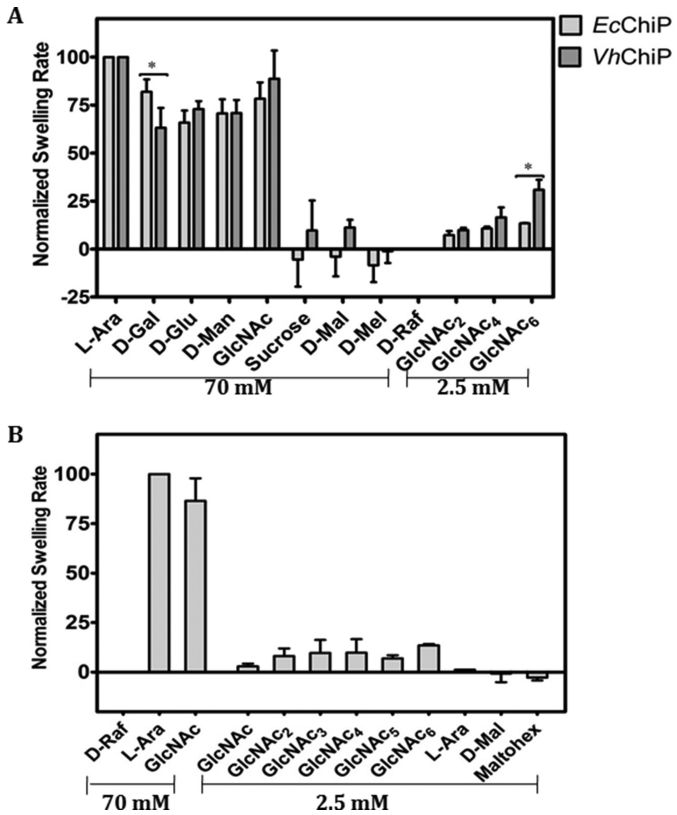

FIGURE 8. **Proteoliposome swelling assays.** In each preparation multilamellar liposomes were reconstituted with 200 ng of *Ec*ChiP or *Vh*ChiP. D-Raffinose was used to determine the isotonic concentrations that produced no change in absorbance at 500 nm of the proteoliposome suspension over 60s. The swelling rate in L-arabinose was set to 100% to obtain normalized swelling rates. The permeability of channels was assumed to be directly proportional to the swelling rate. *A*, permeation of different types of sugar through *Ec*ChiP- and *Vh*ChiP-containing proteoliposomes. Differences between the two data sets were evaluated using a *t* test. Statistically significant differences ($p < 0.05$) are marked with an *asterisk* (*). Values are the means ± S.D., obtained from three-five independent sets of experiments. *B*, permeation of chitooligosaccharides through *Ec*ChiP. Maltodextrins were used as controls. L-Ara, L-arabinose; D-*Gal*, D-galactose; D-*Glu*, D-glucose; D-*Man*, D-mannose; GlcNAc, *N*-acetylglucosamine; D-Mal, D-maltose; D-Mel, D-melezitose; D-*Raf*, D-raffinose; *GlcNAc*$_2$, chitobiose; *GlcNAc*$_3$, chitotriose; *GlcNAc*$_4$, chitotetraose; *GlcNAc*$_5$, chitopentaose; *GlcNAc*$_6$, chitohexaose; *Maltohex*, maltohexaose.

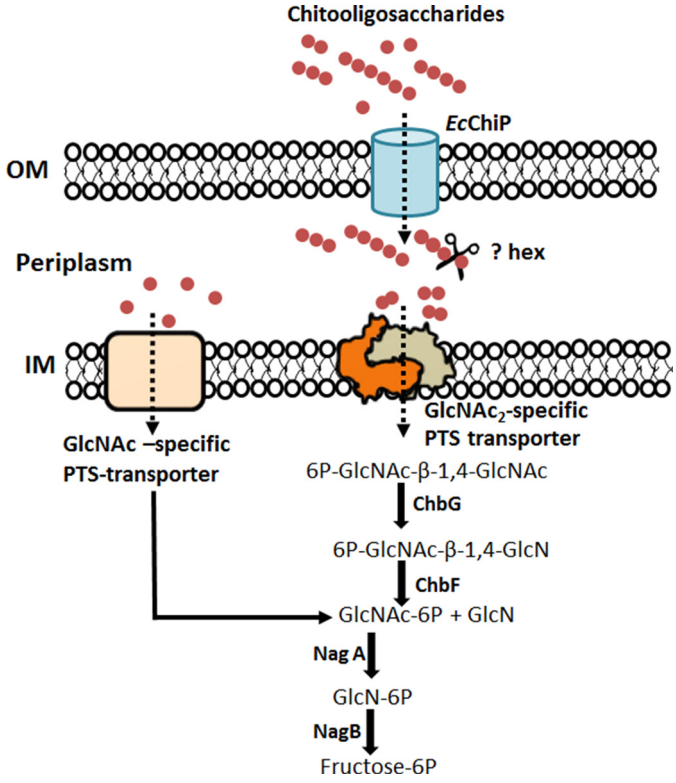

FIGURE 9. **The chitooligosaccharide utilization pathway in *E. coli*.** The scheme is based on the GlcNAc-utilization pathway proposed by Yang *et al.* (14) and Verma and Mahadevan (15). *Solid arrows* denote enzymic reactions, and *dotted arrows* denote the direction of sugar transport. *PTS*, phosphoenolpyruvate transferase system; *OM*, outer membrane; *IM*, inner membrane; *?Hex*, uncharacterized *β-N*-acetylglucosaminidase (EC 3.2.1.96); *ChbG*, chitooligosaccharide monodeacetylase (EC 3.5.1.105); *ChbF*, monoacetyl-chitobiose 6-phosphate hydrolase (EC 3.2.1.86); *NagA*, *N*-acetylglucosamine-6-phosphate deacetylase (EC 3.5.1.25); *NagB*, glucosamine-6-phosphate deaminase (EC 3.5.1.10).

*Ec*ChiP was tested for its ability to transport neutral sugars of various sizes by use of a liposome swelling assay. All the monosaccharides tested could permeate into *Ec*ChiP-reconstituted liposomes. Similar results were obtained with *Vh*ChiP. Neither channel allowed the passage of neutral sugars of >221 Da, such as maltose, sucrose, melezitose, and raffinose, reflecting the size exclusion limit for small molecules that traverse the channel by general diffusion. In our BLM measurements, we did not observe the occlusion of *Ec*ChiP by GlcNAc, presumably because the short-lived blocking events (<100 μs) produced a residence time too short to be resolved by the currently available BLM setup. This is also the case when molecules with a molecular weight below the size exclusion limit pass through the channel without interacting with it. However, the behavior of the *Ec*ChiP channel was not equivalent to that of other known nonspecific porins, such as *Bps*Omp38 from *Burkholderia pseudomallei* (25, 51, 52) and OmpF from *E. coli* (53), which typically have a size exclusion limit of ~650 Da. In liposome swelling experiments, in agreement with the electrophysiological data, *Ec*ChiP showed sugar-selective behavior, allowing the bulk permeation of chitooligosaccharides at rates that depended on the sizes of the sugar chains, longer chain chitooligosaccharides (chitotetraose, pentaose, and hexaose) tending to show greater permeation rates than short chain sugars such as chitobiose and chitotriose. Additionally, the channel operated even at the low sugar concentration of 2.5 mM, a characteristic of solute-specific channels that has been reported for other well characterized porins, including *E. coli* LamB (54, 55) and *V. harveyi* ChiP (8). As shown in Fig. 8*A*, the rate of permeation of chitohexaose through *Vh*ChiP was much greater than those for other sugars, whereas the permeation rates of chitotetraose, pentaose, and hexaose through *Ec*ChiP were comparable. Both the liposome swelling assays and the BLM data generally showed the lower affinity of *Ec*ChiP than of *Vh*ChiP for the same sugars, and suggested high substrate specificity of the *Vibrio* channel and broad substrate specificity of the *E. coli* channel. This is not surprising, as *Vh*ChiP uses chitin as its sole source of energy, so the channel has evolved to provide every efficient chitooligosaccharide uptake, enabling the bacterium to thrive even in rough seas. On the other hand, *E. coli* uses mainly glucose as a nutrient, its ChiP functioning only under certain environmental conditions, such as a scarcity of glucose in the growth medium.

Taking all of our data together, we reconstructed the chitooligosaccharide utilization pathway of *E. coli* based on the GlcNAc utilization pathway suggested previously (14, 15). As shown in Fig. 9, *E. coli* chitoporin facilitates the uptake of extracellular chitooligosaccharides into the periplasm. The breakdown of high molecular weight chitosugars (chitotriose, chitotetraose, chitopentaose, and chitohexaose) within the periplasm may be initiated by an uncharacterized β-*N*-acetylglucosaminidase (Hex), yielding GlcNAc and $GlcNAc_2$. In the subsequent step GlcNAc is transported through the inner membrane by a GlcNAc-specific phosphoenolpyruvate transferase system transporter, forming GlcNAc-6-phosphate, whereas $GlcNAc_2$ is transported and phosphorylated by the ($GlcNAc_2$)-specific enzyme II permease of a different phosphoenolpyruvate transferase system. Utilization of chitobiose is further mediated by the Chb-BCARFG gene products of the Chb operon (56–58). The deacetylase ChbG removes one acetyl group from chitobiose-6-phosphate, generating monoacetyl chitobiose-6-phosphate, which is then the substrate for a β-glucosidase, ChbF. Its product, GlcNAc 6-phosphate (15), is deacetylated to GlcN 6-phosphate by NagA and then deaminated by NagB to fructose 6-phosphate. This final product of the pathway is metabolized as a carbon source for the bacterial cells. In conclusion, our study is the first elucidation of the physiological function of the OprD-like ChiP and provides an insight into how non-chitinolytic bacteria can utilize chitin as an alternative source of cellular energy during the scarcity of glucose-rich nutrients.

Author Contributions—H. S. M. S. designed, performed, and analyzed all the experiments and co-wrote the paper. WS conceived, designed, and coordinated the study and co-wrote and revised the paper.

Acknowledgments—We acknowledge the Biochemistry Laboratory of the Center for Scientific and Technological Equipment and Suranaree University of Technology for providing all research facilities. We greatly appreciate critical proofreading of this manuscript by Dr. David Apps, Centre for Integrative Physiology, School of Biomedical Sciences, University of Edinburgh, United Kingdom.

References

1. Kim, B. H., and Gadd, G. M. (2008) *Bacterial Physiology and Metabolism*, Cambridge University Press, Cambridge, New York
2. Francetic, O., Belin, D., Badaut, C., and Pugsley, A. P. (2000) Expression of the endogenous type II secretion pathway in *Escherichia coli* leads to chitinase secretion. *EMBO J.* **19,** 6697–6703
3. Francetic, O., Badaut, C., Rimsky, S., and Pugsley, A. P. (2000) The ChiA (YheB) protein of *Escherichia coli* K-12 is an endochitinase whose gene is negatively controlled by the nucleoid-structuring protein H-NS. *Mol. Microbiol.* **35,** 1506–1517
4. Suginta, W., Chuenark, D., Mizuhara, M., and Fukamizo, T. (2010) Novel β-*N*-acetylglucosaminidases from *Vibrio harveyi* 650: cloning, expression, enzymatic properties, and subsite identification. *BMC Biochem.* **11,** 40
5. Li, X., and Roseman, S. (2004) The chitinolytic cascade in *Vibrios* is regulated by chitin oligosaccharides and a two-component chitin catabolic sensor/kinase. *Proc. Natl. Acad. Sci. U.S.A.* **101,** 627–631
6. Keyhani, N. O., Li, X. B., and Roseman, S. (2000) Chitin catabolism in the marine bacterium *Vibrio furnissii*: identification and molecular cloning of a chitoporin. *J. Biol. Chem.* **275,** 33068–33076
7. Suginta, W., Chumjan, W., Mahendran, K. R., Janning, P., Schulte, A., and Winterhalter, M. (2013) Molecular uptake of chitooligosaccharides through chitoporin from the marine bacterium *Vibrio harveyi*. *PLoS ONE* **8,** e55126
8. Suginta, W., Chumjan, W., Mahendran, K. R., Schulte, A., and Winterhalter, M. (2013) Chitoporin from *Vibrio harveyi*, a channel with exceptional sugar specificity. *J. Biol. Chem.* **288,** 11038–11046
9. Meekrathok, P., and Suginta, W. (2016) Probing the catalytic mechanism of *Vibrio harveyi* GH20 β-*N*-acetylglucosaminidase by chemical rescue. *PLoS ONE* **11,** e0149228
10. Suginta, W., and Sritho, N. (2012) Multiple roles of Asp-313 in the refined catalytic cycle of chitin degradation by *Vibrio harveyi* chitinase A. *Biosci. Biotechnol. Biochem.* **76,** 2275–2281
11. Sritho, N., and Suginta, W. (2012) Role of Tyr-435 of *Vibrio harveyi* chitinase A in chitin utilization. *Appl. Biochem. Biotechnol.* **166,** 1192–1202
12. Biswas, S., Van Dijck, P., and Datta, A. (2007) Environmental sensing and signal transduction pathways regulating morphopathogenic determinants of *Candida albicans*. *Microbiol. Mol. Biol. Rev.* **71,** 348–376
13. Boulanger, A., Déjean, G., Lautier, M., Glories, M., Zischek, C., Arlat, M., and Lauber, E. (2010) Identification and regulation of the *N*-acetylglucosamine utilization pathway of the plant pathogenic bacterium *Xanthomonas campestri*s pv. campestris. *J. Bacteriol.* **192,** 1487–1497
14. Yang, C., Rodionov, D. A., Li, X., Laikova, O. N., Gelfand, M. S., Zagnitko, O. P., Romine, M. F., Obraztsova, A. Y., Nealson, K. H., and Osterman, A. L. (2006) Comparative genomics and experimental characterization of *N*-acetylglucosamine utilization pathway of *Shewanella oneidensis*. *J. Biol. Chem.* **281,** 29872–29885
15. Verma, S. C., and Mahadevan, S. (2012) The chbG gene of the chitobiose (chb) operon of *Escherichia coli* encodes a chitooligosaccharide deacetylase. *J. Bacteriol.* **194,** 4959–4971
16. Rasmussen, A. A., Johansen, J., Nielsen, J. S., Overgaard, M., Kallipolitis, B., and Valentin-Hansen, P. (2009) A conserved small RNA promotes silencing of the outer membrane protein YbfM. *Mol. Microbiol.* **72,** 566–577
17. Peri, K. G., Goldie, H., and Waygood, E. B. (1990) Cloning and characterization of the *N*-acetylglucosamine operon of *Escherichia coli*. *Biochem. Cell Biol.* **68,** 123–137
18. Figueroa-Bossi, N., Valentini, M., Malleret, L., Fiorini, F., and Bossi, L. (2009) Caught at its own game: regulatory small RNA inactivated by an inducible transcript mimicking its target. *Genes Dev.* **23,** 2004–2015
19. Valentin-Hansen, P., Johansen, J., and Rasmussen, A. A. (2007) Small RNAs controlling outer membrane porins. *Curr. Opin. Microbiol.* **10,** 152–155
20. Vogel, J., and Papenfort, K. (2006) Small non-coding RNAs and the bacterial outer membrane. *Curr. Opin. Microbiol.* **9,** 605–611
21. Plumbridge, J., Bossi, L., Oberto, J., Wade, J. T., and Figueroa-Bossi, N. (2014) Interplay of transcriptional and small RNA-dependent control mechanisms regulates chitosugar uptake in *Escherichia coli* and *Salmonella*. *Mol. Microbiol.* **92,** 648–658
22. Robert, X., and Gouet, P. (2014) Deciphering key features in protein structures with the new ENDscript server. *Nucleic Acids Res.* **42,** W320–W324
23. Montal, M., and Mueller, P. (1972) Formation of bimolecular membranes from lipid monolayers and a study of their electrical properties. *Proc. Natl. Acad. Sci. U.S.A.* **69,** 3561–3566
24. Yoshimura, F., and Nikaido, H. (1985) Diffusion of beta-lactam antibiotics through the porin channels of *Escherichia coli* K-12. *Antimicrob. Agents Chemother.* **27,** 84–92
25. Aunkham, A., Schulte, A., Winterhalter, M., and Suginta, W. (2014) Porin involvement in cephalosporin and carbapenem resistance of *Burkholderia pseudomallei*. *PLoS ONE* **9,** e95918
26. Takanao, S., Honma, S., Miura, T., Ogawa, C., Sugimoto, H., Suzuki, K., and Watanabe, T. (2014) Construction and basic characterization of deletion mutants of the genes involved in chitin utilization by *Serratia marcescens* 2170. *Biosci. Biotechnol. Biochem.* **78,** 524–532
27. Meibom, K. L., Li, X. B., Nielsen, A. T., Wu, C. Y., Roseman, S., and Schoolnik, G. K. (2004) The *Vibrio cholerae* chitin utilization program. *Proc. Natl. Acad. Sci. U.S.A.* **101,** 2524–2529
28. Biswas, S., Mohammad, M. M., Patel, D. R., Movileanu, L., and van den Berg, B. (2007) Structural insight into OprD substrate specificity. *Nat. Struct. Mol. Biol.* **14,** 1108–1109
29. Wang, Y. F., Dutzler, R., Rizkallah, P. J., Rosenbusch, J. P., and Schirmer, T.

(1997) Channel specificity: structural basis for sugar discrimination and differential flux rates in maltoporin. *J. Mol. Biol.* **272,** 56–63
30. Forst, D., Welte, W., Wacker, T., and Diederichs, K. (1998) Structure of the sucrose-specific porin ScrY from *Salmonella typhimurium* and its complex with sucrose. *Nat. Struct. Biol.* **5,** 37–46
31. Conlan, S., Zhang, Y., Cheley, S., and Bayley, H. (2000) Biochemical and biophysical characterization of OmpG: A monomeric porin. *Biochemistry* **39,** 11845–11854
32. van den Berg, B. (2012) Structural basis for outer membrane sugar uptake in pseudomonads. *J. Biol. Chem.* **287,** 41044–41052
33. Strop, P., and Brunger, A. T. (2005) Refractive index-based determination of detergent concentration and its application to the study of membrane proteins. *Protein Sci.* **14,** 2207–2211
34. Saravolac, E. G., Taylor, N. F., Benz, R., and Hancock, R. E. (1991) Purification of glucose-inducible outer membrane protein OprB of *Pseudomonas putida* and reconstitution of glucose-specific pores. *J. Bacteriol.* **173,** 4970–4976
35. Benz, R., Schmid, A., and Vos-Scheperkeuter, G. H. (1987) Mechanism of sugar transport through the sugar-specific LamB channel of *Escherichia coli* outer membrane. *J. Membr. Biol.* **100,** 21–29
36. Ranquin, A., and Van Gelder, P. (2004) Maltoporin: sugar for physics and biology. *Res. Microbiol.* **155,** 611–616
37. Kullman, L., Winterhalter, M., and Bezrukov, S. M. (2002) Transport of maltodextrins through maltoporin: a single-channel study. *Biophys. J.* **82,** 803–812
38. Bezrukov, S. M., Kullman, L., and Winterhalter, M. (2000) Probing sugar translocation through maltoporin at the single channel level. *FEBS Lett.* **476,** 224–228
39. Schwarz, G., Danelon, C., and Winterhalter, M. (2003) On translocation through a membrane channel via an internal binding site: kinetics and voltage dependence. *Biophys. J.* **84,** 2990–2998
40. Zobell, C. E., and Rittenberg, S. C. (1938) The occurrence and characteristics of chitinoclastic bacteria in the sea. *J. Bacteriol.* **35,** 275–287
41. Bassler, B. L., Yu, C., Lee, Y. C., and Roseman, S. (1991) Chitin utilization by marine bacteria: degradation and catabolism of chitin oligosaccharides by *Vibrio furnissii*. *J. Biol. Chem.* **266,** 24276–24286
42. Bassler, B. L., Gibbons, P. J., Yu, C., and Roseman, S. (1991) Chitin utilization by marine bacteria: chemotaxis to chitin oligosaccharides by *Vibrio furnissii*. *J. Biol. Chem.* **266,** 24268–24275
43. Yu, C., Lee, A. M., Bassler, B. L., and Roseman, S. (1991) Chitin utilization by marine bacteria: a physiological function for bacterial adhesion to immobilized carbohydrates. *J. Biol. Chem.* **266,** 24260–24267
44. Keyhani, N. O., and Roseman, S. (1999) Physiological aspects of chitin catabolism in marine bacteria. *Biochim. Biophys. Acta* **1473,** 108–122
45. Park, J. K., Keyhani, N. O., and Roseman, S. (2000) Chitin catabolism in the marine bacterium *Vibrio furnissii*. Identification, molecular cloning, and characterization of a *N,N′*-diacetylchitobiose phosphorylase. *J. Biol. Chem.* **275,** 33077–33083
46. Hunt, D. E., Gevers, D., Vahora, N. M., and Polz, M. F. (2008) Conservation of the chitin utilization pathway in the *Vibrionaceae*. *Appl. Environ. Microbiol.* **74,** 44–51
47. Pruzzo, C., Vezzulli, L., and Colwell, R. R. (2008) Global impact of *Vibrio cholerae* interactions with chitin. *Environ. Microbiol.* **10,** 1400–1410
48. Chumjan, W., Winterhalter, M., Schulte, A., Benz, R., and Suginta, W. (2015) Chitoporin from the marine bacterium *Vibrio harveyi*: probing the essential roles of trp136 at the surface of the constriction zone. *J. Biol. Chem.* **290,** 19184–19196
49. Danelon, C., Brando, T., and Winterhalter, M. (2003) Probing the orientation of reconstituted maltoporin channels at the single-protein level. *J. Biol. Chem.* **278,** 35542–35551
50. Bhamidimarri, S. P., Prajapati, J. D., van den Berg, B., Winterhalter, M., and Kleinekathöfer, U. (2016) Role of electroosmosis in the permeation of neutral molecules: CymA and cyclodextrin as an example. *Biophys. J.* **110,** 600–611
51. Siritapetawee, J., Prinz, H., Krittanai, C., and Suginta, W. (2004) Expression and refolding of Omp38 from *Burkholderia pseudomallei* and *Burkholderia thailandensis* and its function as a diffusion porin. *Biochem. J.* **384,** 609–617
52. Siritapetawee, J., Prinz, H., Samosornsuk, W., Ashley, R. H., and Suginta, W. (2004) Functional reconstitution, gene isolation, and topology modelling of porins from *Burkholderia pseudomallei* and Burkholderia thailandensis. *Biochem. J.* **377,** 579–587
53. Saint, N., Lou, K. L., Widmer, C., Luckey, M., Schirmer, T., and Rosenbusch, J. P. (1996) Structural and functional characterization of OmpF porin mutants selected for larger pore size. II: functional characterization. *J. Biol. Chem.* **271,** 20676–20680
54. Dumas, F., Koebnik, R., Winterhalter, M., and Van Gelder, P. (2000) Sugar transport through maltoporin of *Escherichia coli*: role of polar tracks. *J. Biol. Chem.* **275,** 19747–19751
55. Van Gelder, P., Dumas, F., Rosenbusch, J. P., and Winterhalter, M. (2000) Oriented channels reveal asymmetric energy barriers for sugar translocation through maltoporin of *Escherichia coli*. *Eur. J. Biochem.* **267,** 79–84
56. Keyhani, N. O., Bacia, K., and Roseman, S. (2000) The transport/phosphorylation of *N,N′*-diacetylchitobiose in *Escherichia coli*: characterization of phospho-IIB(Chb) and of a potential transition state analogue in the phosphotransfer reaction between the proteins IIA(Chb) AND IIB-(Chb). *J. Biol. Chem.* **275,** 33102–33109
57. Keyhani, N. O., Boudker, O., and Roseman, S. (2000) Isolation and characterization of IIAChb, a soluble protein of the enzyme II complex required for the transport/phosphorylation of *N,N′*-diacetylchitobiose in *Escherichia coli*. *J. Biol. Chem.* **275,** 33091–33101
58. Keyhani, N. O., Wang, L. X., Lee, Y. C., and Roseman, S. (2000) The chitin disaccharide, N,N′-diacetylchitobiose, is catabolized by *Escherichia coli* and is transported/phosphorylated by the phosphoenolpyruvate:glycose phosphotransferase system. *J. Biol. Chem.* **275,** 33084–33090